Journal of
Materials Chemistry C

Model for the Electro-mechanical Behavior of Elastic Organic Transistors

Journal:	*Journal of Materials Chemistry C*
Manuscript ID	TC-ART-03-2020-001181.R1
Article Type:	Paper
Date Submitted by the Author:	19-May-2020
Complete List of Authors:	Reynolds, Veronica; University of California Santa Barbara, Materials Oh, Saejin; University of California Santa Barbara, Xie, Renxuan; University of California Santa Barbara, Materials Chabinyc, Michael; University of California Santa Barbara, Materials Department; Materials Department

SCHOLARONE™
Manuscripts

Model for the Electro-mechanical Behavior of Elastic Organic Transistors

Veronica Reynolds,[1] Saejin Oh,[2] Renxuan Xie,[1] Michael Chabinyc[1]

[1]Materials Department, University of California, Santa Barbara, 93106

[2]Department of Chemistry and Biochemistry, University of California, Santa Barbara, 93106

Abstract

Organic thin film transistors (TFTs) can be made with materials that allow them to be mechanically stretched during electrical operation. We describe the application of mechanical models of the elasticity of polymers to predict the electrical characteristics of elastic TFTs. The model predicts the current-voltage behavior of TFTs under uniaxial and biaxial deformation assuming stretchable elements for contacts, dielectrics, and the semiconducting layer. The behavior of complementary inverters using elastic TFTs is presented along with criteria for stable operation as digital circuit elements. The mechanical model was also applied to organic electrochemical transistors (OECTs). The behavior of elastic OECTs differs substantially from TFTs and the model predicts that they can provide benefits for the stability of simple digital circuits.

Introduction

The mechanical properties of polymers significantly differ from inorganic materials providing potential advantages for unconventional electronic devices.[1,2] In contrast to inorganic semiconductors that can only be deformed elastically with strains of a few percent, polymers can be deformed to many times their initial dimensions.[3,4] Despite this potential, developing mechanically stretchable semiconducting polymers, dielectrics, and conductors for stretchable electronic devices is a challenge.[5–7] There have been a number of demonstrations of stretchable thin film transistors (TFTs) and circuits with good performance upon deformation.[8–12] These advances demonstrate the need for models for the expected electro-mechanical behavior of stretchable TFTs that can be used to understand their operation.

Here we describe the application of mechanical models of the elasticity of polymer networks[3,4] to predict the electrical behavior of elastic TFTs. We consider TFTs under uniaxial and biaxial deformation assuming stretchable elements for contacts, dielectrics, and the semiconducting layer. Comparison of the expectations for TFTs and organic electrochemical transistors (OECTs) are also presented. Our model shows that in addition to the development of new materials for stretchable electronics there is a pressing need for the development of circuit designs that maintain their functionality under mechanical deformation.

The majority of semiconducting polymers have limited mechanical elasticity relative to insulating elastomers. A material in the elastic regime recovers its initial dimensions after removal of an applied stress. A material that is stretchable can either recover its initial dimensions or plastically deform after removal of an applied stress.[13] The mechanical behavior of polymers depends on their structural order and the temperature relative to their glass transition temperature, T_g. The molecular structure of most high-performance semiconducting polymers leads to a

relatively high T_g (e.g. above ~30° C) and semicrystallinity.[1,14] Poly(3-hexylthiophene), a widely used semiconducting polymer, undergoes plastic deformation without full recovery above strains of ~10%.[15–17] In contrast, simple elastomers are polymer chains crosslinked into a network that exhibit elastic behavior to high strain (>100%) at temperatures above their T_g.[4] Block copolymers, such as styrene-butadiene-styrene (SBS), can also have elastic behavior where some regions are hardened, either by crystallization or by being below their T_g.[13] It is reasonable to believe that semiconducting polymers can be designed to have elastic properties considering that amorphous semiconducting polymers, such as poly(triarylamines), are known.[18–20] Additionally, recent work suggests a design rule for side chain alkylation of conjugated backbones that would lead to intrinsically stretchable semiconductors that operate around room temperature (*i.e.*, $T_g \leq 0$ °C).[21] These side chains can be part of long branched groups on select monomers (not on every ring) to avoid crystallization, or inducing an additional T_g for the side chain itself, thus further improving stretchability and elasticity.

The emergence of composites of semiconductors, or conductors, with elastic polymers has enabled exploration of the behavior of stretchable TFTs and circuits.[22] For example, phase-separated blends of semiconducting polymers and elastomers provide a means to form an elastic semiconducting channel. In blends with elastomers such as poly(dimethylsiloxane) (PDMS) and polystyrene-block-poly(ethylene-co-butylene)-block-polystyrene (SEBS), phase-separated fiber-like aggregates of semiconducting polymers below their T_g accommodate deformation by bending and stretching within the elastic matrix.[10,22–25] Such blends can have effective carrier mobilities in TFTs near 1 $cm^2V^{-1}s^{-1}$ depending on the composition and processing.[24] Single wall carbon nanotubes (SWCNTs) supported by SEBS allow for stretchable electrode materials without overly large injection barriers to organic semiconductors.[7] The mechanical recovery of these composites

is imperfect, but the associated device characteristics of TFTs show intriguing resilience to deformation.[2,24]

Despite efforts to form stretchable electronics, there has not been significant investigation into basic models for the electrical behavior of elastic, or stretchable, TFTs. Without a clear device model that predicts current-voltage characteristics of TFTs with deformation, it is difficult to understand the behavior of novel materials and device structures. Given the questions of non-idealities on the extraction of carrier mobility of polymers from TFTs in conventional devices,[26–28] it is particularly important to understand the expectations for their limiting behavior. Here using a standard model for the mechanical behavior of elastic polymers, we examine the expectations for the current-voltage characteristics of TFTs and OECTs (**Figure 1**). The model provides predictions for the behavior of TFTs deformed by both uniaxial and biaxial stresses as a function of direction with respect to the geometry of the device.

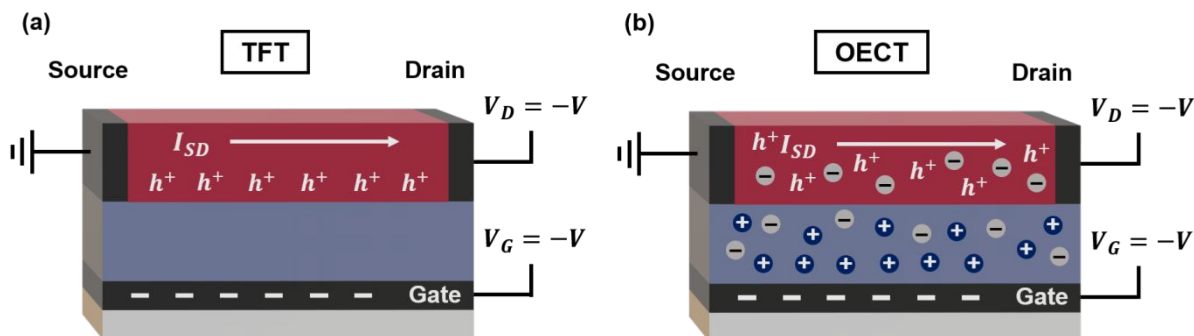

Figure 1. Schematic of a *p*-type **(a)** TFT and **(b)** OECT. Holes, h^+, accumulate and flow at the semiconductor-dielectric interface in the former whereas holes accumulate in the bulk of the semiconductor in the latter due to infiltration of ions from the electrolyte gate.

Results and Discussion

Elastic Thin Film Transistors. The electrical behavior of elastic TFTs can be modeled in the simplest form using the gradual channel model for the current-voltage (*I-V)* characteristics. The gradual channel model for a TFT with carrier mobility (μ), a gate capacitance per area (C_G), a channel width (W), and a channel length (L) is given by Eq. 1 in the linear regime and Eq. 2 in the saturation regime where the source-drain bias (V_{SD}) exceeds the magnitude of the difference between the gate to source voltage (V_G) and a threshold voltage (V_T).[26,28]

$$I_{SD} = \frac{W}{L} C_G \mu \left[\left(V_G - V_T \right) V_{SD} - \frac{V_{SD}^2}{2} \right] \qquad \left| V_{SD} \right| < \left| \left(V_G - V_T \right) \right| \tag{1}$$

$$I_{SD} = \frac{W}{L} C_G \mu \left[\frac{(V_G - V_T)^2}{2} \right] \qquad |V_{SD}| \geq |(V_G - V_T)| \tag{2}$$

The geometry of the TFT along with the coordinate system used for the deformations is given in **Figure 2**. If elastic materials are used for the electrodes, semiconductor, and dielectric then the changes of the *I-V* characteristics of a TFT as a function of deformation can be derived under assumptions about the mechanical and electrical properties of the materials.

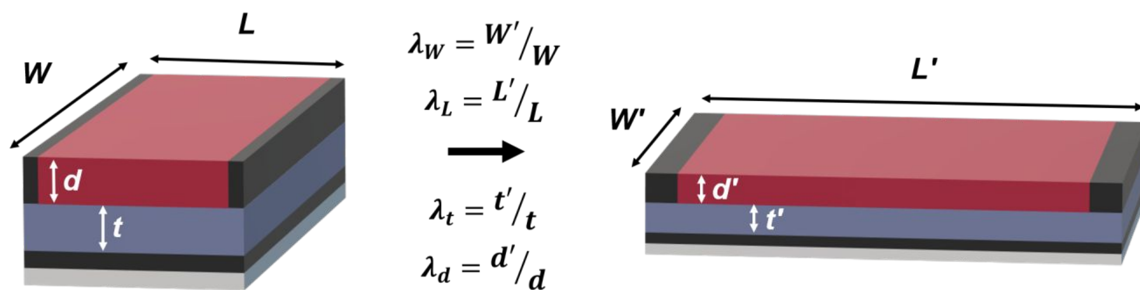

Figure 2. Schematic of the deformation of an elastic TFT with the initial dimensions, final dimensions, and extension ratios, λ, defined.

For the mechanical behavior of the materials in the TFT we assume that the materials are incompressible, i.e. they have Poisson's ratio of 0.5, and are isotropic. Such behavior is an excellent approximation for amorphous polymer networks used as dielectrics.[4,13] For ordered

semiconducting polymers, the assumption of an isotropic response is not necessarily valid because of the mixture of crystalline and disordered regions, but we expect that it should hold for amorphous semiconducting polymers. We also assume that electrodes made from composites, e.g SWCNTs supported by or blended in SEBS, will follow this behavior as well. For polymers that undergo high deformation it is common to define an extension ratio, λ, rather than strain. The extension ratio is defined as the ratio of the deformed dimension (x_i') to its initial dimension (x_i) in a particular direction, *i,* and is given by $\lambda_i = x_i'/x_i$. Here we model the TFT using a deformation along the channel direction, λ_L, along the width, λ_W, in the thickness of the semiconducting layer, λ_d, and in the thickness of the dielectric layer, λ_t. With Poisson's ratio of 0.5, the product of the extension ratios is unity, i.e. $\lambda_W\lambda_L\lambda_t = 1$.[4] We assume that deformation throughout the TFT is uniform, i.e. the channel, dielectric, and electrodes have equivalent deformation (although the mechanical stress in each layer might be different due to differences in mechanical moduli). We also assume the TFT is free to move in all directions other than that of the applied deformation. Note that this assumption can be invalidated in practice if a TFT is not deformed in a controlled fashion, e.g. in true uniaxial or biaxial strain.

For the electrical properties of the materials in the TFT, we make several important assumptions. The dielectric constant of the gate dielectric is modeled as independent of deformation, which is a reasonable assumption assuming the chain dimensions are not strongly perturbed. We also assume that the mobility of the semiconductor does not vary with extension; this assumption is reasonable for an amorphous polymer at deformations that do not strongly perturb the chain dimensions relative to the initial state. At high extension ($\lambda >> 1$), changes in the mobility are expected because the polymer chains extend which could lead to variations in the transport pathways and the energetic disorder.[15] We also assume that the accumulation layer is

sufficiently thin, e.g. ~1 nm, relative to the thickness of the undeformed semiconductor that the change in dimension does not affect the operation of the device. Our model does not incorporate the role of contact resistances in transistors, which are ignored in the basic gradual channel model, and we comment on the potential effects for various cases of deformations below.

Uniaxial Deformation of TFTs. The first case for the electrical behavior with deformation is simple uniaxial extension or compression either along the direction of the channel or across it. The full derivation of the model is given in the Supplementary Information and we highlight here the most critical factors. The gate capacitance can be shown to vary as $\sqrt{\lambda} C_G$ with uniaxial deformation along the channel length, or the width, therefore under compression the capacitance will decrease and under extension it will increase. We model change in V_T of the TFT by assuming that the amount of trapped charge per area, q_{trap}, does not change with deformation. In this case, V_T will be a function of C_G because $q_{trap} = V_T C_G$ (assuming that the device turns on in the sub-threshold regime near V_G=0 V). The expression for the current in the saturation region for change in channel dimensions W and L is given by Equation 3 for deformation along the channel direction and Equation 4 for deformation across the channel with comparable expressions for the linear regime (see Supporting Information).

$$I_{SD} = \frac{1}{\lambda_L} \frac{W}{L} C_G \mu \left[\frac{1}{2} \left(V_G - \frac{1}{\sqrt{\lambda_L}} V_T \right)^2 \right] \quad (3)$$

$$I_{SD} = \lambda_W{}^2 \frac{W}{L} C_G \mu \left[\frac{1}{2} \left(V_G - \frac{1}{\sqrt{\lambda_W}} V_T \right)^2 \right] \quad (4)$$

The effect of uniaxial deformation is strikingly different in the two cases despite the similar modification of V_T. The relative current ($I_{SD,\lambda}/I_{SD,\lambda=1}$) in the saturation regime upon deformation of a model *p*-type TFT with W/L=1, C_G=5 nF/cm^2, and $V_T = -10$ V and $V_G = -40$ V is shown in **Figure 3**. Because the mobility is constant, it does not impact the relative current. The current scales as $\sim 1/\lambda_L$, at small V_T relative to V_G, as the device is stretched along the channel length, L, because the change in the width and thickness of the dielectric compensate each other. The current scales as $\sim \lambda_W{}^2$ for extension along the channel width, W, due to the shortening of the channel length and the decrease in thickness of the gate dielectric. This result also holds for the saturation regime at small V_T relative to V_G (see Supplementary Information). It can be seen from the plots that deformation along the channel length produces a smaller change in the output current of the TFT than deformation along the channel width; note that if the *I-V* characteristics are plotted on a log scale to show the on-to-off characteristic then such changes would be more difficult to see than in the case where the deformation is along the width of the TFT.

As a TFT undergoes deformation, the resistance of the channel will change. As the channel length increases the current drops under the condition of a vanishingly small contact resistance. However, in practical organic TFTs the contact resistance may be comparable to the channel resistance depending on the initial dimensions of the device, i.e. for short channel lengths or if there is a substantial injection barrier.[28] Upon extension, the channel resistance increases leading to a smaller influence of a fixed contact resistance as the device is stretched along L, but has an increasing effect upon compression as the channel resistance drops. The change in channel

resistance differs with deformation along *W* and could, in principle, lead to apparent differences in mobility extracted from a device with a contact resistance that is competitive with the channel resistance. Given that contact resistances are known to strongly influence the extraction of the apparent carrier mobility in high performance TFTs,[26,28] the best practice would be to evaluate the contact resistance using a variety of channel lengths before interpreting changes in mobility upon deformation. One expects that larger devices, e.g. $L > 100$ µm, would be preferable for studies of the elastic behavior of TFTs particularly without reasonable models of the injection barrier using elastic conducting composites as electrodes.

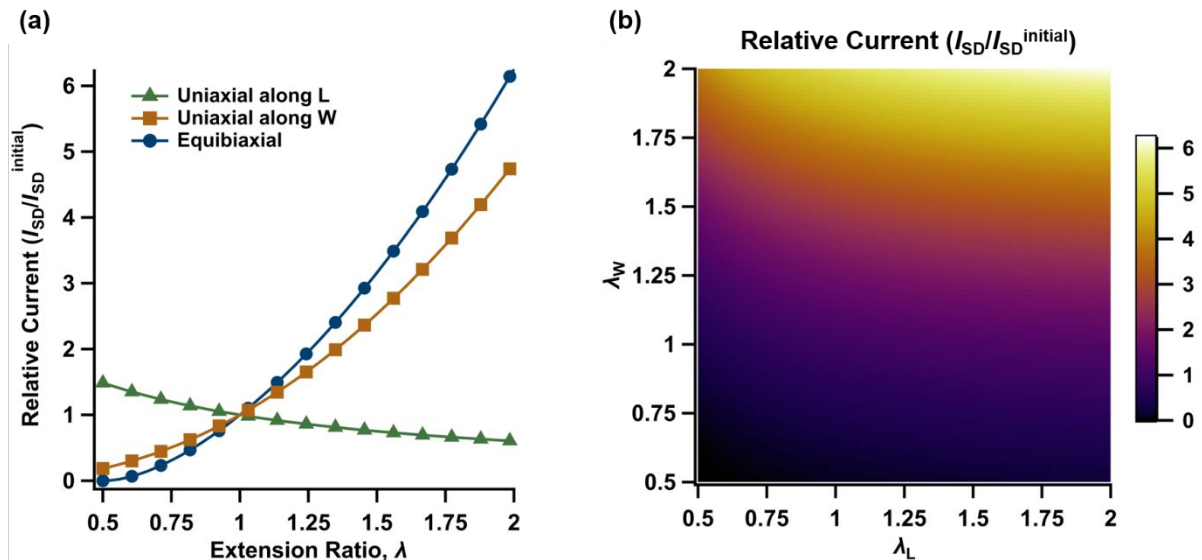

Figure 3. (a) Relative I_{SD} of a TFT in the saturation regime as a function of extension ratio for uniaxial deformation along *L* (triangles) and *W* (squares) and equi-biaxial deformation along *L* and *W* (circles). **(b)** Two-dimensional plot of the relative current for biaxial deformation. The TFT was modeled with the following parameters: $W/L=1$, $C_G=5 \times 10^{-9}$ F/cm^2, and a $V_T=-10$ V with $V_G=-40$ V.

Biaxial Extension. If a TFT is deformed along both the width and length of the channel in biaxial deformation, Eq. 5 shows that the current in the saturation regime scales with $\sim\lambda_W^2$. This behavior can be understood by considering the changes under biaxial extension. The thickness of the dielectric changes as the product $1/\lambda_W\lambda_L$ thereby modifying the gate capacitance. This change compensates for the change in L and the device outputs a current that is surprisingly dominated by changes in W at high V_G relative to V_T despite the biaxial deformation. The relative current with deformation for the case of equi-biaxial deformation along L and W is given in **Figure 3a** and that for the full spectrum of biaxial deformation is given in **Figure 3b**

$$I_{SD} = \lambda_W^{\ 2} \frac{W}{L} C_G \mu \left[\frac{1}{2} \left(V_G - \frac{1}{\lambda_L \lambda_W} V_T \right)^2 \right] \tag{5}$$

A striking prediction of the model is that if the device is compressed then the effective V_T could increase enough to shut the TFT off. Given the assumption in the model that shifts in V_T are dominated by the change in the gate capacitance, this condition occurs when $V_T/V_G = \lambda_L\lambda_W$. The switch to the off-state could occur at relatively low compression of both directions, e.g. $\lambda\sim0.7$, at low values of V_G and suggests that such TFTs would be highly sensitive to deformation near this operational condition.

Comparisons to Literature. We can compare the model to some results reported in literature, however we note that no truly elastic semiconducting polymers have been reported to our knowledge. The most widely studied stretchable TFTs use composites to achieve elastic behavior. The apparent mobility of stretchable TFTs formed with SEBS/(diketopyrrolopyrole-based

semiconducting polymer) blends, SWCNTs supported by SEBS as electrodes, and an SEBS dielectric was reported to be roughly constant based on extraction of the *I-V* characteristics.[2] The current of the TFTs dropped with extension along the channel length in agreement with the model here, but was nearly constant with deformation along the width to extension of ~1.75 in contrast to predictions here for uniaxial deformation along *W*.[2] An explanation for the difference would be that the inhomogeneous polymer aggregates in the SEBS matrix did not fill the channel as *W* increased, i.e. the number of semiconducting pathways between the source and drain did not change with deformation in the blend. We can also compare the model to TFTs formed with an elastic PDMS dielectric, PDMS-encapsulated SWCNT electrodes, and amorphous indacenodithiophene-*co*-benzodiathiazole polymer (IDTBT). These TFTs show a decrease in current with extension along *L*, but a more complex behavior with extension along *W* where the current decreases then increases again.[29] The apparent mobility of the TFT was reported to decrease with deformation in both directions; this could arise from changes in the morphology of the semiconductor or potentially a change in injection from the SWCNT composite electrodes. Considering that the gate capacitance of SEBS dielectrics does change as expected by the model,[24] detailed analysis of stretchable TFTs using the model here should help to reveal the physical origin of changes in the *I-V* characteristics.

Predictions for the behavior of circuits. The model for the *I-V* characteristics of TFTs with deformation also shows that the layout of a circuit with respect to the deformation direction will have a significant impact on the performance of a stretchable circuit. We consider the case of a complementary inverter with *n*- and *p*-type TFTs with the physical layouts shown in **Figure 4**. In digital circuits inverters are used to change the sign of the input voltage, V_{in}, as an output voltage,

V_{out}.[30] In analog circuits the inverter can be used as a simple amplifier when operated near an input value referred to as the inverting voltage, V_{inv}, where both the *n*- and *p*-type TFTs are in saturation (see **Figure S1**).[30] Complementary inverters made with organic TFTs have been studied to understand the impacts of gate bias stress and other factors on their operation.[31,32]

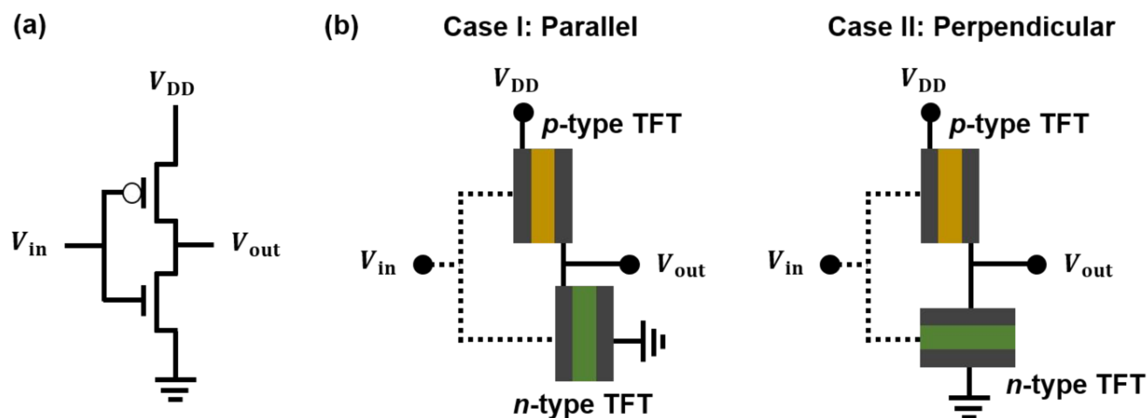

Figure 4. **(a)** Diagram of a complementary inverter circuit with *n*- and *p*-type TFTs. V_{DD} is the supply voltage. **(b)** Top view of the physical layouts of an inverter circuit where the channels of the TFTs are oriented parallel to each other (Case I) and perpendicular to each other (Case II). The dashed line indicates connections to the gate electrodes of the TFTs.

In Case I the TFTs are arranged such that deformation affects both devices in the same way whereas in Case II the TFTs are laid out perpendicular to each other. The operation of circuits

such as inverters depends on changes in the resistance, i.e. I_{SD}, of the TFTs upon deformation, which occur even if the mobility of the semiconductor is constant. For Case I, a stability criterion for V_{inv} can be derived from the behavior as a function of uniaxial extension. Eq. 6 gives the expected value of V_{inv} with deformation along L (see Supporting Information for derivation).

$$V_{inv} = \frac{V_{DD} - \frac{1}{\sqrt{\lambda_L}}\left|V_{T,p}\right| + \frac{1}{\sqrt{\lambda_L}} V_{T,n}\sqrt{\beta_n / \beta_p}}{1 + \sqrt{\beta_n / \beta_p}} \quad (6)$$

In these expressions, β is equal to $(W/L)\mu C_G$ for the *n*- and *p*-type TFTs. Eq. 7 gives the resulting stability criterion such that V_{inv} is invariant with λ_L that forces the dimensions of the *n*- and *p*-type TFTs to be set by the ratio of V_T for the *n*- and *p*-type TFTs (Eq. 7). This expression is valid for deformation along W with substitution of λ_W for λ_L because the behavior depends only on the change in V_T with deformation. Here we ignore changes in V_T due to gate bias stress which has been considered previously and depends on the functional form of the shift in V_T.[31]

$$\sqrt{\beta_n / \beta_p} = \frac{\left|V_{T,p}\right|}{V_{T,n}} \quad (7)$$

In contrast to Case I, no stability criterion can be found in Case II because the dimensions of the two TFTs change differently with extension. Here V_{inv} is given by Eq. 8 in this case for deformation, λ, along the channel of the *p*-type TFT and the width of the *n*-type TFT.

$$V_{inv} = \frac{V_{DD} - \frac{1}{\sqrt{\lambda}}\left|V_{T,p}\right| + \frac{1}{\sqrt{\lambda}}V_{T,n}\lambda^{3/2}\sqrt{\beta_n/\beta_p}}{1 + \lambda^{3/2}\sqrt{\beta_n/\beta_p}} \quad (8)$$

Figure 5 shows the inverter characteristics in both Case I and II along with a plot of V_{inv} with *n*- and *p*- TFTs with device parameters comparable to typical TFTs with polymeric gate dielectrics. For both cases the gain (the slope near V_{inv}) varies with deformation with the most severe changes occurring for Case II. In both cases, if the input voltage is well away from V_{inv}, the circuit will still operate as an inverter, but the operational window is substantially affected by deformation in Case II. Such characteristics will lead to a relatively poor noise margin in complex circuits.[30–32] The model does show that if the mechanical deformation is predictable, e.g. for a circuit in a device that is constrained to stretch along a particular direction, then circuits and driving voltages may be designed to compensate for mechanical strain. Additionally, the behavioral predictions from the model can be used to design high sensitivity strain/pressure sensors with built-in response, such as the Case II layout, in which V_{inv} varies significantly with deformation. More complex circuit layouts with multiple inverters can potentially be designed to detect and deconvolute strains in multiple directions.

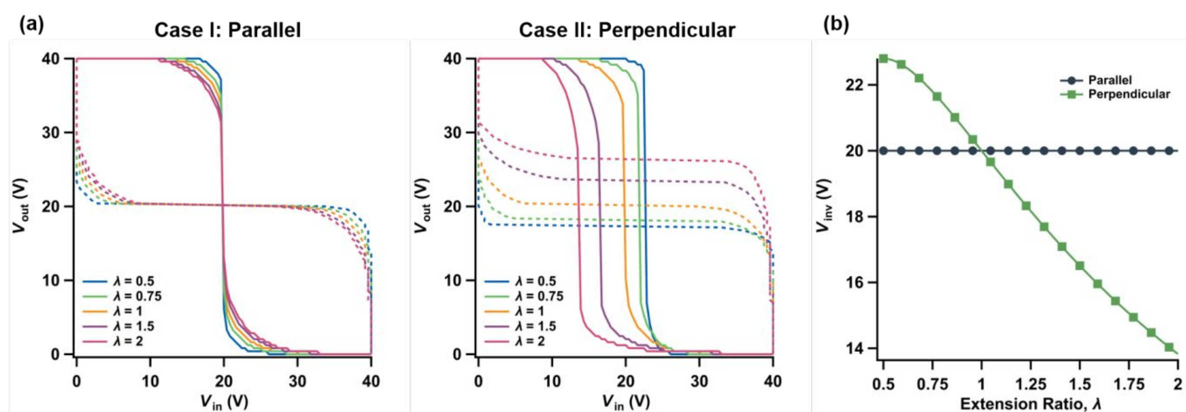

Figure 5. (a) Characteristics for an inverter with the Case I and Case II layouts as described in Figure 4. The solid line shows the output voltage, V_{out}, with respect to the input voltage, V_{in}, and the dashed lines are transformations of the circuit performance to highlight the eye of the operational regime of the circuit. **(b)** Inverting voltage, V_{inv}, with deformation for Case I and Case II showing stability when the TFTs are oriented in the same direction with respect to the deformation and instability when they are not.

Elastic Electrochemical Transistors. In addition to TFTs, other types of transistors known as organic electrochemical double layer transistors (EDLTs) and organic electrochemical transistors (OECTs) are under investigation.[33–35] In contrast to TFTs, the gate dielectric in EDLTs and OECTs is formed from a fluid or solid-state electrolyte with mobile ions that respond to the gate voltage. In OECTs the current of the transistor flows through the bulk of the semiconducting layer due to infiltration of ions into the semiconductor (**Figure 1**), but in EDLTs ions cannot infiltrate the semiconductor and current flows at the surface of the semiconductor. These devices have advantages over conventional organic TFTs because the operating voltages are low due to the high

capacitance of the ionic dielectric. OECTs in particular are being examined widely in bioelectronics because of their high transconductance.[36]

We can model EDLTs and OECTs with similar assumptions to TFTs, but with a few key differences. We assume that the capacitance of the electrochemical gate is not affected by deformation because the motion of ions to form the double layer, or to penetrate the bulk, should be relatively insensitive to the thickness of the dielectric. The model should be valid for both solid-state electrolytes and for solvent-based electrolytes. We note that we have ignored the effect of swelling of the semiconductor by the ions, which is typically small (a few percent change in volume);[37,38] however for precise modeling at small deformations such changes should be considered as well. The model predicts the *I-V* behavior at steady state and ignores the speed of the formation of the EDL or the kinetics of infiltration of ions into the channel in an OECT.[36,39,40] We also note that in EDLT and OECT devices parasitic capacitances can play a significant role as well due to the large double layer capacitance of the dielectric. These effects will also be modified by deformation due to changes in the area of the electrodes,[40] but we ignore those effects because they are very specific to the exact device design and here only focus on the limiting behavior where the TFT channel controls the operation.

In the case of an EDLT, charge is accumulated in a thin layer of the semiconductor at the interface of the dielectric and semiconductor due to formation of an electrochemical double layer. Dimensional changes in the thickness of the semiconductor are not a factor in the operation of EDLTs. For uniaxial deformation, the current of the EDLT varies more strongly than for the TFT because of differences in the behavior of the dielectric. Eq. 9 and Eq. 10 give the results for the *I-V* behavior in the saturation regime upon uniaxial deformation along L and W, respectively. Here there is no dependence of the V_T upon deformation assuming no change in the trap density because

of the constant C_G. Under biaxial strain, the change in I_{SD} depends only on the ratio of the deformations along L and W leading to stable operation with equal biaxial deformation (Eq. 11).

$$I_{SD} = \frac{1}{\lambda_L^{3/2}} \frac{W}{L} C_G \mu \left[\frac{(V_G - V_T)^2}{2} \right] \tag{9}$$

$$I_{SD} = \lambda_W^{3/2} \frac{W}{L} C_G \mu \left[\frac{(V_G - V_T)^2}{2} \right] \tag{10}$$

$$I_{SD} = \frac{\lambda_W}{\lambda_L} \frac{W}{L} C_G \mu \left[\frac{(V_G - V_T)^2}{2} \right] \tag{11}$$

The current in OECTs between the source and drain depends on the thickness of the semiconducting layer, d, because it flows through the bulk due to infiltration of ions from the gate dielectric. Models for the detailed I-V characteristics of OECTs are under investigation and here we use the simplest case where a volumetric capacitance of the semiconductor, C^*, determines I_{SD} with applied gate bias.[35] C^* is determined by the carriers per volume in the semiconductor and is limited for a given material by the number of repeat units in the polymer, i.e. there are a maximum number of valence (or conduction) electrons that can be removed (added) to the polymer. We assume that C^* is unaffected by deformation, which is reasonable because there is no change in monomers per volume. The I-V behavior of an OECT in saturation is given by Eq. 11 where d is the thickness of the semiconducting layer.

$$I_{SD} = \frac{W}{L} dC^* \mu \left[\frac{(V_G - V_T)^2}{2} \right] \tag{11}$$

Upon deformation the resistance of the OECT changes with the dimensions of the semiconductor. The conduction through the bulk of the semiconductor leads to a fixed V_T because we assume that the number of trap states does not change with deformation. Given these assumptions, the expectations for the *I-V* behavior in the saturation regime with uniaxial deformation along L and W and biaxial deformation are given by Eq. 12, 13, and 14. Comparable expressions will hold for the linear regime of operation.

$$I_{SD} = \frac{1}{\lambda_L^2} \frac{W}{L} dC^* \mu \left[\frac{(V_G - V_T)^2}{2} \right] \tag{12}$$

$$I_{SD} = \lambda_W \frac{W}{L} dC^* \mu \left[\frac{(V_G - V_T)^2}{2} \right] \tag{13}$$

$$I_{SD} = \frac{1}{\lambda_L^2} \frac{W}{L} dC^* \mu \left[\frac{(V_G - V_T)^2}{2} \right] \tag{14}$$

The variation in the current for OECTs can be seen in **Figure 6** where both uniaxial and biaxial deformation leads to substantial changes in the current. Due to the scaling of the dimensions, the

biaxial case (Eq. 14) shows no dependence on λ_W because of the constraint from the thickness of the semiconductor.

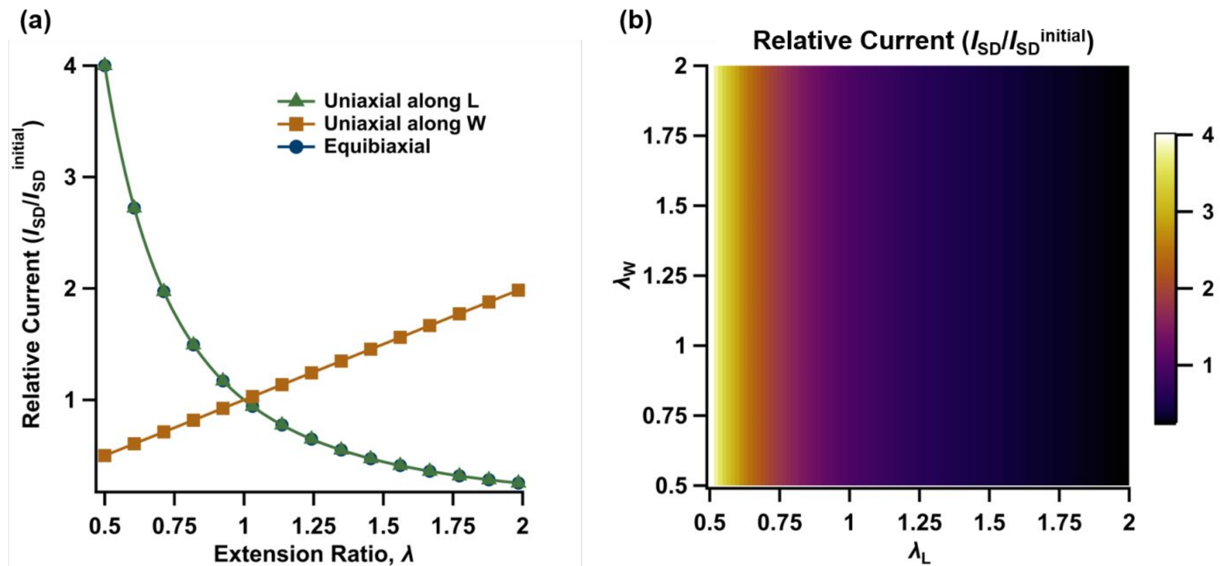

Figure 6. (a) Relative I_{SD} of an OECT in the saturation regime as a function of extension ratio for uniaxial deformation along *L* (triangles) and *W* (squares) and equibiaxial deformation along *L* and *W* (circles). **(b)** Two-dimensional plot of the relative current for biaxial deformation. The OECT was modeled with the following parameters: W/L=1, C^*=40 F/cm^3, d = 100 nm, and V_T=−0.5 V with V_G = −3 V.

The model allows us to determine if there are potential advantages of OECTs vs. TFTs for elastic circuits. First, OECTs have lower operating voltages than TFTs and the current can be

much higher than TFTs because of the conduction through the bulk of the device.[34] For current-driven circuits, such as an organic light emitting diode (OLED) connected to an OECT, the output current varies substantially upon deformation and would lead to significant changes in the operation, e.g. brightness, of an OLED. In contrast, for a digital circuit like a complementary inverter, it is possible to find conditions where the dimensions of the TFTs can be set to provide a stable value of V_{inv} with deformation for both Case I and Case II (see Supporting Information). The predicted behavior of OECT-based inverters with respect to deformation is given in Figure 7. The condition for a stable inverter is the same in both cases because of the assumption in the model that V_T is independent of deformation. This would suggest that for some digital circuits the layout of OECTs relative to the deformation direction could be more forgiving than for conventional TFTs. Note that we have not considered the frequency-dependent behavior of OECTs where the kinetics of ion motion could couple with mechanical motion which could be a fruitful area to pursue for unique electrical behavior for sensing. The overall results suggest that elastic OECTs are worth pursuing for circuit applications and could have unique behavior relative to TFTs.

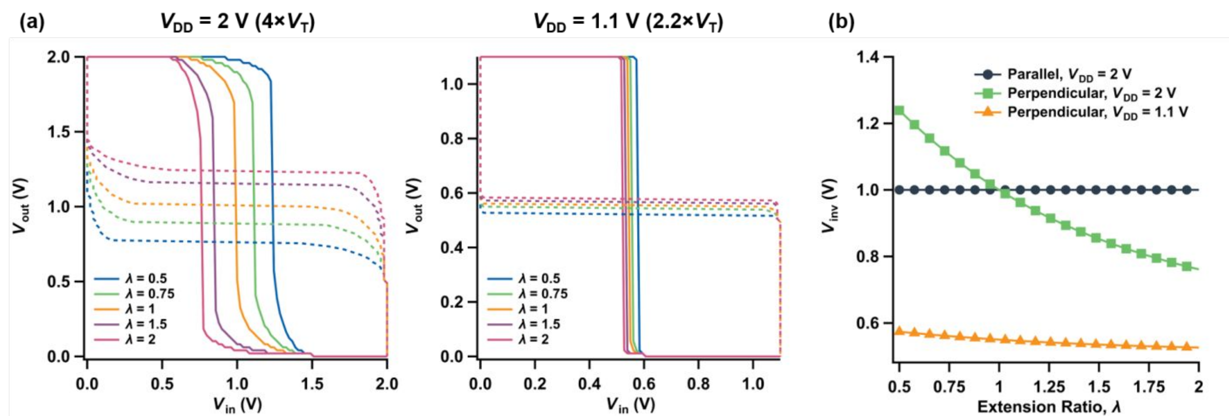

Figure 7. (a) Characteristics for an OECT inverter with the Case II (perpendicular) layout, with two different supply voltages: 2 V (farther from the stability criterion) and 1.1 V (closer to the stability criterion). **(b)** Inverting voltage, V_{inv}, with deformation for Case I and Case II (at the two different supply voltages) showing higher stability for the Case II device operated near the stability criterion.

Summary

A model for the electro-mechanical behavior of elastic TFTs was derived under assumptions of uniform deformation of the semiconductor, dielectric, and electrodes that have the mechanical behavior of incompressible elastic polymer networks. While the model is simple, it provides a means to interpret changes in the electrical operation of TFTs with deformation. Both conventional and electrochemical TFTs are predicted to show substantial changes in their I_{SD} with deformation due to changes in the dimensions of the channel and dielectric. This behavior should be considered in the physical layout of stretchable circuits along with the mechanical strains that the circuit may experience under operation.

Many reports of stretchable TFTs focus on the mobility of the semiconducting material, but the behavior of circuits strongly depends on changes in the absolute resistance of the circuit elements with deformation. The negative effects of strain have been noted for silicon-based circuits[41] and led to the design of rigid TFTs with stretchable interconnects that have a negligible contribution to the circuit operation.[42,43] If fully stretchable electronics are desired, then circuit designs that are less sensitive to precise current levels and shifts in V_T will be essential. Some neuromorphic elements and designs, such as Schmitt triggers,[44] can compensate for variation in changes in input voltages and such designs may prove to be important for elastic organic devices. Because the behavior of elastic TFTs and OECTs differ substantially upon deformation, improved models of the *I-V* behavior of OECTs will benefit the design of future bioelectronic systems. We also expect that new materials and circuit designs for stretchable electronics could lead to improved performance in sensing where the physical behavior of the material is used beneficially.

Acknowledgement. This work was supported by the National Science Foundation through the MRSEC Program of the National Science Foundation through Grant No. DMR-1720256 (IRG-2). V.G.R. was partially supported by the National Science Foundation Graduate Research Fellowship Program. We thank Prof. Tse Nga Ng (UC San Diego) for helpful conversations.

References

(1) Root, S. E.; Savagatrup, S.; Printz, A. D.; Rodriquez, D.; Lipomi, D. J. Mechanical Properties of Organic Semiconductors for Stretchable, Highly Flexible, and Mechanically Robust Electronics. *Chem. Rev.* **2017**, *117* (9), 6467–6499. https://doi.org/10.1021/acs.chemrev.7b00003.

(2) Wang, S.; Xu, J.; Wang, W.; Wang, G.-J. N.; Rastak, R.; Molina-Lopez, F.; Chung, J. W.; Niu, S.; Feig, V. R.; Lopez, J.; Lei, T.; Kwon, S.-K.; Kim, Y.; Foudeh, A. M.; Ehrlich, A.; Gasperini, A.; Yun, Y.; Murmann, B.; Tok, J. B.-H.; Bao, Z. Skin Electronics from Scalable Fabrication of an Intrinsically Stretchable Transistor Array. *Nature* **2018**, *555* (7694), 83–88. https://doi.org/10.1038/nature25494.

(3) Ward, I. M.; Sweeney, J. *Mechanical Properties of Solid Polymers*, Third edition.; Wiley: Chichester, West Sussex, United Kingdom, 2013.

(4) Treloar, L. R. G. *The Physics of Rubber Elasticity: By L.R.G. Treloar*, 3rd ed.; Oxford classic texts in the physical sciences; Clarendon Press ; Oxford University Press: Oxford : New York, 2005.

(5) Kleinschmidt, A. T.; Lipomi, D. J. Stretchable Conjugated Polymers: A Case Study in Topic Selection for New Research Groups. *Acc. Chem. Res.* **2018**, *51* (12), 3134–3143. https://doi.org/10.1021/acs.accounts.8b00459.

(6) Kong, D.; Pfattner, R.; Chortos, A.; Lu, C.; Hinckley, A. C.; Wang, C.; Lee, W.-Y.; Chung, J. W.; Bao, Z. Capacitance Characterization of Elastomeric Dielectrics for Applications in Intrinsically Stretchable Thin Film Transistors. *Adv. Funct. Mater.* **2016**, *26* (26), 4680–4686. https://doi.org/10.1002/adfm.201600612.

(7) Matsuhisa, N.; Chen, X.; Bao, Z.; Someya, T. Materials and Structural Designs of Stretchable Conductors. *Chem. Soc. Rev.* **2019**, *48* (11), 2946–2966. https://doi.org/10.1039/C8CS00814K.

(8) Cai, L.; Zhang, S.; Miao, J.; Yu, Z.; Wang, C. Fully Printed Stretchable Thin-Film Transistors and Integrated Logic Circuits. *ACS Nano* **2016**, *10* (12), 11459–11468. https://doi.org/10.1021/acsnano.6b07190.

(9) Zhang, G.; McBride, M.; Persson, N.; Lee, S.; Dunn, T. J.; Toney, M. F.; Yuan, Z.; Kwon, Y.-H.; Chu, P.-H.; Risteen, B.; Reichmanis, E. Versatile Interpenetrating Polymer Network Approach to Robust Stretchable Electronic Devices. *Chem. Mater.* **2017**, *29* (18), 7645–7652. https://doi.org/10.1021/acs.chemmater.7b03019.

(10) Kim, H.-J.; Thukral, A.; Sharma, S.; Yu, C. Biaxially Stretchable Fully Elastic Transistors Based on Rubbery Semiconductor Nanocomposites. *Adv. Mater. Technol.* **2018**, *3* (6), 1800043. https://doi.org/10.1002/admt.201800043.

(11) Oh, J. Y.; Rondeau-Gagné, S.; Chiu, Y.-C.; Chortos, A.; Lissel, F.; Wang, G.-J. N.; Schroeder, B. C.; Kurosawa, T.; Lopez, J.; Katsumata, T.; Xu, J.; Zhu, C.; Gu, X.; Bae, W.-G.; Kim, Y.; Jin, L.; Chung, J. W.; Tok, J. B.-H.; Bao, Z. Intrinsically Stretchable and Healable Semiconducting Polymer for Organic Transistors. *Nature* **2016**, *539* (7629), 411–415. https://doi.org/10.1038/nature20102.

(12) Kang, B.; Song, E.; Lee, S. B.; Chae, B.-G.; Ahn, H.; Cho, K. Stretchable Polymer Gate Dielectric with Segmented Elastomeric Network for Organic Soft Electronics. *Chem. Mater.* **2018**, *30* (18), 6353–6360. https://doi.org/10.1021/acs.chemmater.8b02388.

(13) Strobl, G. *The Physics of Polymers*; Springer Berlin Heidelberg: Berlin, Heidelberg, 2007. https://doi.org/10.1007/978-3-540-68411-4.

(14) Lang, A. S.; Muth, M.-A.; Heinrich, C. D.; Carassco-Orozco, M.; Thelakkat, M. Pendant Perylene Polymers with High Electron Mobility. *J. Polym. Sci. Part B Polym. Phys.* **2013**, *51* (20), 1480–1486. https://doi.org/10.1002/polb.23357.
(15) O'Connor, B.; Kline, R. J.; Conrad, B. R.; Richter, L. J.; Gundlach, D.; Toney, M. F.; DeLongchamp, D. M. Anisotropic Structure and Charge Transport in Highly Strain-Aligned Regioregular Poly(3-Hexylthiophene). *Adv. Funct. Mater.* **2011**, *21* (19), 3697–3705. https://doi.org/10.1002/adfm.201100904.
(16) Moulton, J.; Smith, P. Electrical and Mechanical Properties of Oriented Poly(3-Alkylthiophenes): 2. Effect of Side-Chain Length. *Polymer* **1992**, *33* (11), 2340–2347. https://doi.org/10.1016/0032-3861(92)90525-2.
(17) Koch, F. P. V.; Rivnay, J.; Foster, S.; Müller, C.; Downing, J. M.; Buchaca-Domingo, E.; Westacott, P.; Yu, L.; Yuan, M.; Baklar, M.; Fei, Z.; Luscombe, C.; McLachlan, M. A.; Heeney, M.; Rumbles, G.; Silva, C.; Salleo, A.; Nelson, J.; Smith, P.; Stingelin, N. The Impact of Molecular Weight on Microstructure and Charge Transport in Semicrystalline Polymer Semiconductors–Poly(3-Hexylthiophene), a Model Study. *Prog. Polym. Sci.* **2013**, *38* (12), 1978–1989. https://doi.org/10.1016/j.progpolymsci.2013.07.009.
(18) Thelakkat, M.; Hagen, J.; Haarer, D.; Schmidt, H.-W. Poly(Triarylamine)s- Synthesis and Application in Electroluminescent Devices and Photovoltaics. *Synth. Met.* **1999**, *102* (1–3), 1125–1128. https://doi.org/10.1016/S0379-6779(98)01412-X.
(19) Zhang, W.; Smith, J.; Hamilton, R.; Heeney, M.; Kirkpatrick, J.; Song, K.; Watkins, S. E.; Anthopoulos, T.; McCulloch, I. Systematic Improvement in Charge Carrier Mobility of Air Stable Triarylamine Copolymers. *J. Am. Chem. Soc.* **2009**, *131* (31), 10814–10815. https://doi.org/10.1021/ja9034818.
(20) Aitken, B. S.; Wieruszewski, P. M.; Graham, K. R.; Reynolds, J. R.; Wagener, K. B. Control of Charge-Carrier Mobility via In-Chain Spacer Length Variation in Sequenced Triarylamine Functionalized Polyolefins. *ACS Macro Lett.* **2012**, *1* (2), 324–327. https://doi.org/10.1021/mz2001725.
(21) Xie, R.; Weisen, A. R.; Lee, Y.; Aplan, M. P.; Fenton, A. M.; Masucci, A. E.; Kempe, F.; Sommer, M.; Pester, C. W.; Colby, R. H.; Gomez, E. D. Glass Transition Temperature from the Chemical Structure of Conjugated Polymers. *Nat. Commun.* **2020**. https://doi.org/doi:10.1038/s41467-020-14656-8.
(22) Song, E.; Kang, B.; Choi, H. H.; Sin, D. H.; Lee, H.; Lee, W. H.; Cho, K. Stretchable and Transparent Organic Semiconducting Thin Film with Conjugated Polymer Nanowires Embedded in an Elastomeric Matrix. *Adv. Electron. Mater.* **2016**, *2* (1), 1500250. https://doi.org/10.1002/aelm.201500250.
(23) Shin, M.; Song, J. H.; Lim, G.-H.; Lim, B.; Park, J.-J.; Jeong, U. Highly Stretchable Polymer Transistors Consisting Entirely of Stretchable Device Components. *Adv. Mater.* **2014**, *26* (22), 3706–3711. https://doi.org/10.1002/adma.201400009.
(24) Xu, J.; Wang, S.; Wang, G.-J. N.; Zhu, C.; Luo, S.; Jin, L.; Gu, X.; Chen, S.; Feig, V. R.; To, J. W. F.; Rondeau-Gagné, S.; Park, J.; Schroeder, B. C.; Lu, C.; Oh, J. Y.; Wang, Y.; Kim, Y.-H.; Yan, H.; Sinclair, R.; Zhou, D.; Xue, G.; Murmann, B.; Linder, C.; Cai, W.; Tok, J. B.-H.; Chung, J. W.; Bao, Z. Highly Stretchable Polymer Semiconductor Films through the Nanoconfinement Effect. *Science* **2017**, *355* (6320), 59–64. https://doi.org/10.1126/science.aah4496.
(25) Shin, M.; Oh, J. Y.; Byun, K.-E.; Lee, Y.-J.; Kim, B.; Baik, H.-K.; Park, J.-J.; Jeong, U. Polythiophene Nanofibril Bundles Surface-Embedded in Elastomer: A Route to a Highly

Stretchable Active Channel Layer. *Adv. Mater.* **2015**, *27* (7), 1255–1261. https://doi.org/10.1002/adma.201404602.

(26) Choi, H. H.; Cho, K.; Frisbie, C. D.; Sirringhaus, H.; Podzorov, V. Critical Assessment of Charge Mobility Extraction in FETs. *Nat. Mater.* **2018**, *17* (1), 2–7. https://doi.org/10.1038/nmat5035.

(27) McCulloch, I.; Salleo, A.; Chabinyc, M. Avoid the Kinks When Measuring Mobility. *Science* **2016**, *352* (6293), 1521–1522. https://doi.org/10.1126/science.aaf9062.

(28) Paterson, A. F.; Singh, S.; Fallon, K. J.; Hodsden, T.; Han, Y.; Schroeder, B. C.; Bronstein, H.; Heeney, M.; McCulloch, I.; Anthopoulos, T. D. Recent Progress in High-Mobility Organic Transistors: A Reality Check. *Adv. Mater.* **2018**, *30* (36), 1801079. https://doi.org/10.1002/adma.201801079.

(29) Zheng, Y.; Wang, G. N.; Kang, J.; Nikolka, M.; Wu, H.; Tran, H.; Zhang, S.; Yan, H.; Chen, H.; Yuen, P. Y.; Mun, J.; Dauskardt, R. H.; McCulloch, I.; Tok, J. B. -H.; Gu, X.; Bao, Z. An Intrinsically Stretchable High-Performance Polymer Semiconductor with Low Crystallinity. *Adv. Funct. Mater.* **2019**, *29* (46), 1905340. https://doi.org/10.1002/adfm.201905340.

(30) Rabaey, J. M. *Digital Integrated Circuits: A Design Perspective*; Prentice Hall electronics and VLSI series; Prentice Hall: Upper Saddle River, N.J, 1996.

(31) Chow, M. J.; Sun, B.; He, Y.; Payne, M. M.; Anthony, J. E.; Li, Y.; Levine, P. M.; Wong, W. S. Transistor Sizing for Bias-Stress Instability Compensation in Inkjet-Printed Organic Complementary Inverters. *IEEE Electron Device Lett.* **2016**, *37* (11), 1438–1441. https://doi.org/10.1109/LED.2016.2614536.

(32) Ng, T.-N.; Sambandan, S.; Lujan, R.; Arias, A. C.; Newman, C. R.; Yan, H.; Facchetti, A. Electrical Stability of Inkjet-Patterned Organic Complementary Inverters Measured in Ambient Conditions. *Appl. Phys. Lett.* **2009**, *94* (23), 233307. https://doi.org/10.1063/1.3153510.

(33) Kim, S. H.; Hong, K.; Xie, W.; Lee, K. H.; Zhang, S.; Lodge, T. P.; Frisbie, C. D. Electrolyte-Gated Transistors for Organic and Printed Electronics. *Adv. Mater.* **2013**, *25* (13), 1822–1846. https://doi.org/10.1002/adma.201202790.

(34) Andersson Ersman, P.; Lassnig, R.; Strandberg, J.; Tu, D.; Keshmiri, V.; Forchheimer, R.; Fabiano, S.; Gustafsson, G.; Berggren, M. All-Printed Large-Scale Integrated Circuits Based on Organic Electrochemical Transistors. *Nat. Commun.* **2019**, *10* (1). https://doi.org/10.1038/s41467-019-13079-4.

(35) Rivnay, J.; Leleux, P.; Ferro, M.; Sessolo, M.; Williamson, A.; Koutsouras, D. A.; Khodagholy, D.; Ramuz, M.; Strakosas, X.; Owens, R. M.; Benar, C.; Badier, J.-M.; Bernard, C.; Malliaras, G. G. High-Performance Transistors for Bioelectronics through Tuning of Channel Thickness. *Sci. Adv.* **2015**, *1* (4), e1400251. https://doi.org/10.1126/sciadv.1400251.

(36) Rivnay, J.; Inal, S.; Salleo, A.; Owens, R. M.; Berggren, M.; Malliaras, G. G. Organic Electrochemical Transistors. *Nat. Rev. Mater.* **2018**, *3* (2). https://doi.org/10.1038/natrevmats.2017.86.

(37) Thomas, E. M.; Brady, M. A.; Nakayama, H.; Popere, B. C.; Segalman, R. A.; Chabinyc, M. L. X-Ray Scattering Reveals Ion-Induced Microstructural Changes During Electrochemical Gating of Poly(3-Hexylthiophene). *Adv. Funct. Mater.* **2018**, *28* (44), 1803687. https://doi.org/10.1002/adfm.201803687.

(38) Giridharagopal, R.; Flagg, L. Q.; Harrison, J. S.; Ziffer, M. E.; Onorato, J.; Luscombe, C. K.; Ginger, D. S. Electrochemical Strain Microscopy Probes Morphology-Induced Variations in Ion Uptake and Performance in Organic Electrochemical Transistors. *Nat. Mater.* **2017**, *16* (7), 737–742. https://doi.org/10.1038/nmat4918.

(39) Said, E.; Larsson, O.; Berggren, M.; Crispin, X. Effects of the Ionic Currents in Electrolyte-Gated Organic Field-Effect Transistors. *Adv. Funct. Mater.* **2008**, *18* (21), 3529–3536. https://doi.org/10.1002/adfm.200701251.

(40) Zare Bidoky, F.; Frisbie, C. D. Parasitic Capacitance Effect on Dynamic Performance of Aerosol-Jet-Printed Sub 2 V Poly(3-Hexylthiophene) Electrolyte-Gated Transistors. *ACS Appl. Mater. Interfaces* **2016**, *8* (40), 27012–27017. https://doi.org/10.1021/acsami.6b08396.

(41) Ahn, J.-H.; Kim, H.-S.; Menard, E.; Lee, K. J.; Zhu, Z.; Kim, D.-H.; Nuzzo, R. G.; Rogers, J. A.; Amlani, I.; Kushner, V.; Thomas, S. G.; Duenas, T. Bendable Integrated Circuits on Plastic Substrates by Use of Printed Ribbons of Single-Crystalline Silicon. *Appl. Phys. Lett.* **2007**, *90* (21), 213501. https://doi.org/10.1063/1.2742294.

(42) Rogers, J. A.; Someya, T.; Huang, Y. Materials and Mechanics for Stretchable Electronics. *Science* **2010**, *327* (5973), 1603–1607. https://doi.org/10.1126/science.1182383.

(43) Lacour, S. P.; Wagner, S.; Narayan, R. J.; Li, T.; Suo, Z. Stiff Subcircuit Islands of Diamondlike Carbon for Stretchable Electronics. *J. Appl. Phys.* **2006**, *100* (1), 014913. https://doi.org/10.1063/1.2210170.

(44) Bubel, S.; Menyo, M. S.; Mates, T. E.; Waite, J. H.; Chabinyc, M. L. Schmitt Trigger Using a Self-Healing Ionic Liquid Gated Transistor. *Adv. Mater.* **2015**, *27* (21), 3331–3335. https://doi.org/10.1002/adma.201500556.

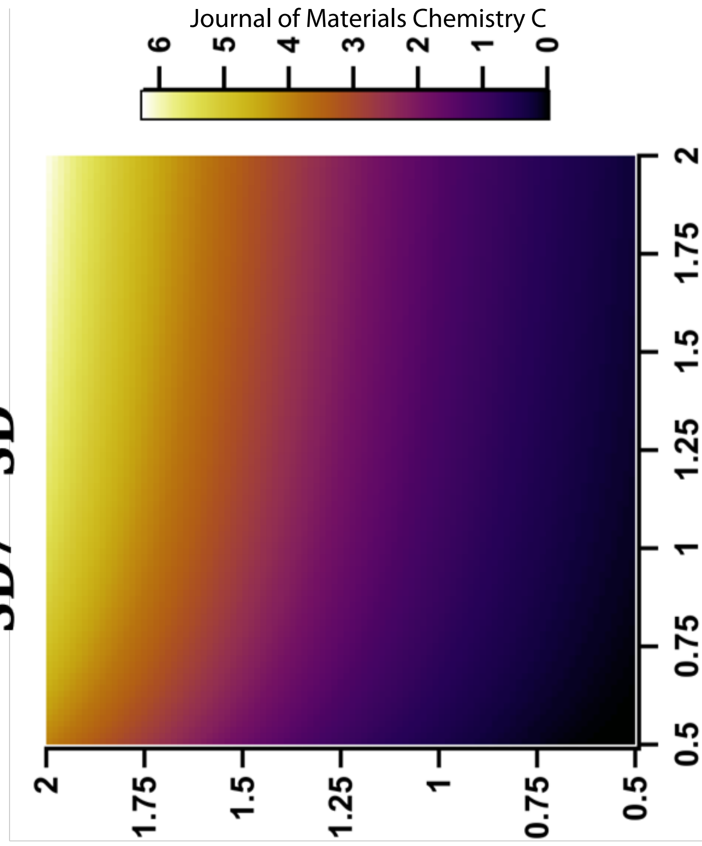

$I_{SD}/I_{SD}^{initial}$
λ_W
λ_L
0.5
0.75
1
1.25
1.5
1.75
2
0
1
2
3
4
5
6

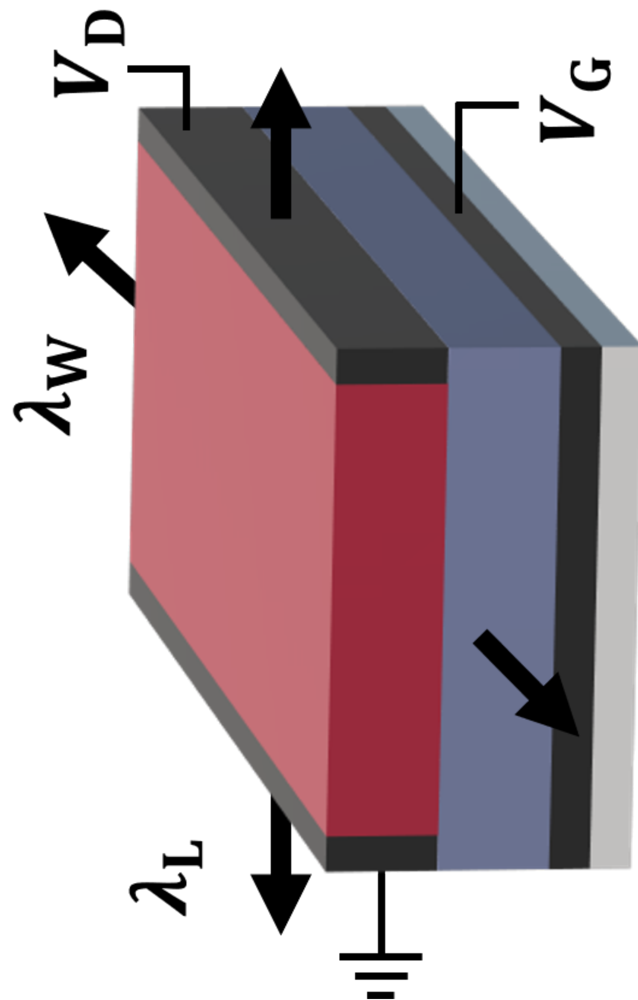

λ_W
λ_L
V_D
V_G